# Weyl semimetals in ultrafast laser fields

Fatemeh Nematollahi, S. Azar Oliaei Motlagh, Vadym Apalkov, and Mark I. Stockman

# Weyl semimetals in ultrafast laser fields

Fatemeh Nematollahi, S. Azar Oliaei Motlagh, Vadym Apalkov, and Mark I. Stockman
*Center for Nano-Optics (CeNO) and Department of Physics and Astronomy,*
*Georgia State University, Atlanta, Georgia 30303, USA*
(Dated: May 30, 2019)

We study theoretically interaction of topological Weyl semimetals with an ultrafast optical pulse. The electron dynamics in such material is coherent and highly anisotropic. For some directions of pulse polarization, the electric dynamics is irreversible, which means that the residual electron conduction band population after the pulse is comparable to the maximum conduction band population during the pulse. For other directions of polarization, the electron dynamics is highly reversible and, after the pulse, the electron system returns to its initial state with almost zero conduction band population. Such high anisotropy in electron dynamics is related to anisotropy in interband dipole matrix elements. In the reciprocal space, the electron conduction band population density shows hot spots near the Weyl points. The optical pulse also causes net charge transfer through the system. The direction of transfer is the same as the direction of the field maximum. The transferred charge has highly anisotropic dependence on polarization direction with almost zero transferred charge for some directions.

## I. INTRODUCTION

Interaction of solids with ultrashort optical pulses has been a subject of intensive theoretical and experimental research[1–13]. For short pulses with the duration of a few femtoseconds, which is less than the characteristics electron scattering time, the electron dynamics is coherent and can be described by a time dependent Schrödinger equation. For strong pulses, the electric field of the pulse is comparable to the internal electric field of a solid. Such pulses can strongly modify both transport and optical properties of solids. It was shown that wide band gap insulators such as quartz, sapphire and calcium floride, regardless of dissimilarity in their physical properties, undergo semimetallization during the pulse, which is observed as a finite charge transfer through an insulator during the pulse[15–18]. For such materials, the electron dynamics during the pulse is highly reversibility, which means that the electron system returns to its initial state after the pulse, i.e., the residual conduction band (CB) population is small. Such reversibility is due to a large band gap, $\triangle \approx 10 eV \gg \hbar\omega$ ($\omega$ is the frequency of the pulse), and smooth dependence of the interband coupling on the reciprocal vector.

For solids with a small band gap, $\Delta \ll \hbar\omega$, the electron dynamics in a strong optical pulse is usually irreversible, which means that the residual CB population is comparable with the maximum CB population during the pulse. Here the residual CB population is defined as the population at the moment when the pulse ends. Such irreversibility of electron dynamics is also due to highly nonuniform interband dipole coupling as a function of a reciprocal vector. In this case the residual CB population distribution in the reciprocal space has patterns that are determined by both polarization of the pulse and the crystal structure of a solid. For example, for 2D materials, such as graphene, silicene/germanene, and phosphorene, the residual CB population shows hot spots in the reciprocal space[20,21,23,24] that are near the Dirac points for graphene and near the $\Gamma$ point for phosphorene. These hot spots are due to singular nature of the interband dipole matrix elements near these points. Such singularity can be also employed to realize the interferometry in graphenes reciprocal space without a magnetic field when a circularly polarized optical pulse is incident on graphene monolayer[22].

Here we study another class of topological systems with singular interband dipole matrix elements. These systems are three dimensional (3D) topological Weyl semimetals. The quasiparticle excitations in such materials are Weyl fermions[25–29] with linear low-energy dispersion relation. Similar to graphene, which also has relativistic low-energy dispersion relation but in 2D, the bulk electron states in Weyl semimetals are chiral. The Weyl nodes in such semimetals come in pairs, which are separated in the reciprocal space and have opposite chirality. We consider interaction of such Weyl fermions with an ultrashort optical pulse and identify the fingerprints of unique dispersion relation of these materials in the conduction band population distribution in the reciprocal space. The Weyl semimetal is a unique system in a sense that it can be considered as a combination of many layers of graphene-like subsystems that are anisotropic and have different bandgaps. Thus, by probing the Weyls semimetals with ultrashort optical pulse we can study the effect of such pulses on anisotpic gapped graphene-like materials. Below we show that the interaction of an ultrashort pulse with Weyl fermions is highly anisotropic and strongly depends on the direction of pulse polarization. In general, the electron dynamics in the field of the pulse is highly irreversible, which is similar to graphene. At the same time, for some directions of polarizations, the electron dynamics is reversible, i.e., after the pulse, the system returns to its initial state. Such behavior is different from graphene and illustrates the fact the reversibil-
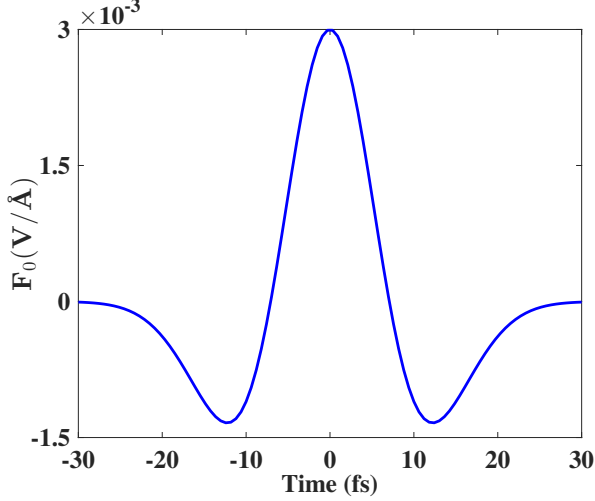
FIG. 1: (Color online) Profile of the optical pulse with $\tau = 10$ fs and $F_0 = 0.003$ V/Å.

ity of electron dynamics is determined by both the magnitude of the bandgap and the properties of the interband dipole coupling.

## II.  MODEL AND MAIN EQUATIONS

We assume that the ultrashort optical pulse has the following form[30]

$$\mathbf{F}(t) = \mathbf{F}_0 e^{-u^2}(1 - 2u^2), \qquad (1)$$

where the direction of the pulse polarization is determined by the direction of vector $\mathbf{F}_0 = (F_{x0}, F_{y0}, F_{z0})$, while the magnitude $F_0$ of this vector is the pulse amplitude, $u = t/\tau$, and $\tau$ is the pulse duration. Below we consider ultrashort pulses with the duration of $\tau = 10$ fs. The profile of such pulse with amplitude $F_0 = 0.003$ (V/Å) is shown in Fig.1.

The time-dependent Hamiltonian of a system in the field of the pulse is given by the following expression

$$\mathcal{H} = \mathcal{H}_0 + e\mathbf{F}(t)\mathbf{r}. \qquad (2)$$

Here $\mathcal{H}_0$ is the field-free electron Hamiltonian, $\mathbf{r}$ is a position vector, and $e$ is an electron charge. For the field-free Hamiltonian we use the lower-energy approximation of the full Hamiltonian of the system in the reciprocal space near the Weyl points. The corresponding Hamiltonian has the following form[31]

$$\mathcal{H}_0 = E_0\mathbb{I} + \mathbf{v}_0.\mathbf{q}.\mathbb{I} + v_x q_x \sigma_x + v_y q_y \sigma_y + v_z q_z \sigma_z, \quad (3)$$

where $\mathbb{I}$ is the identity matrix, $\mathbf{q} = \mathbf{k} - \mathbf{k}_0$, $\mathbf{k}_0$ is the position of the Weyl point in the reciprocal space, $\mathbf{k}$ is the electron wave vector , and $\sigma_i$ are three Pauli matrices. Here $\mathbf{v}_0 = (v_{0,x}, v_{0,y}, v_{0,z})$, $v_x$, $v_y$, $v_z$, and $E_0$ are

the parameters of the Hamiltonian. The corresponding conduction and valence band energy dispersions are the following

$$E_c = \hbar(v_{0x}q_x + v_{0y}q_y + v_{0z}q_z + \sqrt{\mu}) \qquad (4)$$

for the conduction band and

$$E_v = \hbar(v_{0x}q_x + v_{0y}q_y + v_{0z}q_z - \sqrt{\mu}) \qquad (5)$$

for the valence band. Here $\mu = v_x^2 q_x^2 + v_y^2 q_y^2 + v_z^2 q_z^2$. The coherent electron dynamics in the field of the pulse is described by the time dependent Schrödinger equation

$$i\hbar\frac{d\psi}{dt} = \mathcal{H}\psi. \qquad (6)$$

Here the time dependence in the Hamiltonian comes from the time dependent electric field. Such electric field results in both interband and intraband electron dynamics. The intraband electron dynamics, i.e. the dynamics within a single band, is described by the acceleration theorem

$$\hbar\frac{d\mathbf{k}}{dt} = e\mathbf{F}(t), \qquad (7)$$

with the solution of the form

$$\mathbf{k}_T(\mathbf{q}, t) = \mathbf{q} + \frac{e}{\hbar}\int_{-\infty}^{t}\mathbf{F}(t_1)dt_1. \qquad (8)$$

Here $\mathbf{q}$ is the initial wave vector. This solution does not depend on the band index, which means that the intraband dynamics in the reciprocal space is the same for all bands. The corresponding wave functions are Houston functions[32]

$$\Phi_{\alpha q}^{(H)}(\mathbf{r}, t) = \psi_{\mathbf{k}_T(\mathbf{q},t)}^{\alpha}(r)e^{-\frac{i}{\hbar}\int_{-\infty}^{t}dt_1 E_\alpha[\mathbf{k}_T(q,t_1)]}. \qquad (9)$$

Here $\psi_{\mathbf{k}}^{\alpha}(r)$ is the wave function of the field-free Hamiltonian for band $\alpha$. Then the general solution of the Schrödinger equation can be expressed in the basis of Houston functions as

$$\psi_q(\mathbf{r}, t) = \sum_{\alpha=v,c} \beta_{\alpha q}(t)\Phi_{\alpha q}^{(H)}(\mathbf{r}, t), \qquad (10)$$

where $\beta_{\alpha q}(t)$ are expansion coefficients that satisfy the following system of differential equations

$$\frac{d\beta_{cq}}{dt} = -i\frac{\mathbf{F}(t)\mathbf{Q}_q(t)}{\hbar}\beta_{vq}(t), \qquad (11)$$

$$\frac{d\beta_{vq}}{dt} = -i\frac{\mathbf{F}(t)\mathbf{Q}_q^*(t)}{\hbar}\beta_{cq}(t), \qquad (12)$$

where vector function $\mathbf{Q}_q$ are defined by interband dipole matrix elements

$$\mathbf{Q}_q(t) = \mathbf{D}[\mathbf{k}(\mathbf{q}, t)]\exp\left(i[\phi_{cv}^{(B)}(t) + \phi_{cv}^{(D)}(t)]\right), \quad (13)$$

where the dynamic phase is

$$\phi_{cv}^{(D)}(t) = -\frac{1}{\hbar}\int_{-\infty}^{t} dt_1\bigg(E_c[\mathbf{k}(\mathbf{q},t_1)] - E_v[\mathbf{k}(\mathbf{q},t_1)]\bigg),$$
(14)

and the topological (Berry) phase is

$$\phi_{cv}^{(B)}(t) = \frac{e}{\hbar}\int_{-\infty}^{t}\bigg(A_{vv}[\mathbf{k}(\mathbf{q},t_1)] - A_{cc}[\mathbf{k}(\mathbf{q},t_1)]\bigg)\mathbf{F}(t_1)dt_1,$$
(15)

and

$$A_{\alpha\alpha}(\mathbf{k}) = \langle\psi_{\mathbf{k}}^{(\alpha)}|i\frac{\partial}{\partial\mathbf{k}}|\psi_{\mathbf{k}}^{(\alpha)}\rangle,$$
(16)

where $\alpha$ corresponds to the conduction band $c$ and the valence band $v$. The dipole matrix elements between the valence and conduction bands are defined by the following expression

$$\mathbf{D}(\mathbf{k}) = \langle\psi_{\mathbf{k}}^{(c)}|e\mathbf{r}|\psi_{\mathbf{k}}^{(v)}\rangle.$$
(17)

Substituting the wave functions found from the field-free Hamiltonian (3) into Eq. (17), we obtain the following expressions for the dipole matrix elements

$$D_x(\mathbf{k}) = \frac{e}{2i\mu}\frac{-v_x}{\sqrt{v_x^2q_x^2 + v_y^2q_y^2}}\bigg(v_xq_xv_zq_z + iv_yq_y\sqrt{\mu}\bigg),$$

$$D_y(\mathbf{k}) = \frac{e}{2i\mu}\frac{-v_y}{\sqrt{v_x^2q_x^2 + v_y^2q_y^2}}\bigg(v_yq_yv_zq_z - iv_xq_x\sqrt{\mu}\bigg),$$

$$D_z(\mathbf{k}) = \frac{ev_z}{2i\mu}\sqrt{v_x^2q_x^2 + v_y^2q_y^2}.$$
(18)

The system of equations (11)-(12) is solved numerically with the following initial conditions $(\beta_{vq}, \beta_{cq}) = (1, 0)$. This condition means that in the initial state, the valence band is occupied and the conduction band is empty. Then the time dependent conduction band population of a state with wave vector $\mathbf{q}$ is $|\beta_{cq}(t)|^2$, while the total conduction band population is

$$\mathcal{N}_{CB}(t) = \sum_q |\beta_{cq}(t)|^2.$$
(19)

Intraband dynamics combined with electron redistribution between the bands generates an electric current during the pulse, which can be found from the following expression

$$J_j(t) = \frac{e}{(2\pi)^3}\int d\mathbf{q}\sum_{\alpha_1=v,c}\sum_{\alpha_2=vc}\beta_{\alpha_1 q}^*(t)V_j^{\alpha_1\alpha_2}\beta_{\alpha_2 q}(t),$$
(20)

where $j = x, y, z$ and $V_j^{\alpha_1\alpha_2}$ are the matrix elements of the velocity operator,

$$V_j = \frac{1}{\hbar}\frac{\partial H_0}{\partial k_j},$$
(21)

calculated between the valence and conduction band states. These matrix elements are given by the following expressions

$$V_x^{vv} = v_{0x} - \frac{v_x^2q_x}{\sqrt{\mu}}$$
(22)

$$V_x^{cc} = v_{0x} + \frac{v_x^2q_x}{\sqrt{\mu}}$$
(23)

$$V_x^{vc} = V_x^{*cv} = \frac{1}{\sqrt{\mu - v_z^2q_z^2}}\frac{v_x}{\sqrt{\mu}}\bigg(-v_xv_zq_xq_z + i\sqrt{\mu}v_yq_y\bigg)$$
(24)

$$V_y^{vv} = v_{0y} - \frac{v_y^2q_y}{\sqrt{\mu}}$$
(25)

$$V_y^{cc} = v_{0y} + \frac{v_y^2q_y}{\sqrt{\mu}}$$
(26)

$$V_y^{vc} = V_y^{*cv} = \frac{1}{\sqrt{\mu - v_z^2q_z^2}}\frac{v_y}{\sqrt{\mu}}\bigg(-v_yv_zq_yq_z - i\sqrt{\mu}v_yq_y\bigg)$$
(27)

$$V_z^{vv} = v_{0z} - \frac{v_z^2q_z}{\sqrt{\mu}}$$
(28)

$$V_z^{cc} = v_{0z} + \frac{v_z^2q_z}{\sqrt{\mu}}$$
(29)

$$V_z^{vc} = V_z^{cv} = \frac{v_z}{\sqrt{\mu}}\sqrt{\mu - v_z^2q_z^2}$$
(30)

With the known current, we can find the net charge transferred through the system during the pulse

$$Q_{tr,j} = \int_{-\infty}^{\infty} dt J_j(t).$$
(31)

## III. RESULTS AND DISCUSSION

We present the results for TaAs, which has a body-centered tetragonal lattice system, see Fig.2, with lattice constants $a = b = 3.437\mathring{A}$ along $x$ and $y$ direction, respectively and $c = 11.646\mathring{A}$ along $z$ direction. TaAs has two pairs of Weyl points with following coordinates: $(\pm 0.0072, 0.4827, 1.0000)$ for the first pair, $W_1$ and $(\pm 0.0185, 0.2831, 0.6000)$ for the second pair, $W_2$[33]. Here the coordinates of the points are given in units of reciprocal lattice vectors. The parameters of the effective low-energy Hamiltonian (3) can be found from the known velocities in the conduction and valence bands[33]. The corresponding parameters are given in Table 1 for two sets of Weyl points.

The relaxation dynamics of electrons in TaAs, photoexcited by a short pulse, has been studied experimentally in Ref.[7]. It was shown that, after the pulse, the electron relaxation occurs at picosecond time scale, which makes these materials suitable candidates for optical switching. Here we study another aspect of interaction of ultrashort optical pulses with Weyl semimetals.

TABLE I: The parameters (velocities) of effective Hamiltonian (3) in units of $10^5 m/s$ for two sets of Weyl points.

| Velocity | $W_1$ | $W_2$ |
|---|---|---|
| $v_{0x}$ | $-1.35$ | $-0.95$ |
| $v_{0y}$ | $-1$ | $0.9$ |
| $v_{0z}$ | $0$ | $1.35$ |
| $v_x$ | $3.85$ | $3.35$ |
| $v_y$ | $2.2$ | $2.6$ |
| $v_z$ | $0.2$ | $2.95$ |



FIG. 2: (Color online) Body-centered tetragonal structure of TaAs.

Namely, we study the electron dynamics during the pulse. We characterize this dynamics in terms of the total CB population and the distribution of CB population in the reciprocal space. Such distribution is strongly correlated with the profile of the corresponding interband dipole matrix elements.

### A. x-polarized pulse

For the $x$-polarized pulse (the pulse is incident along $z$ direction, see Fig.2) the coupling between the bands is determined by the $x$ component of the interband dipole matrix element, $D_x$. For the first Weyl point, $W_1$, the interband dipole matrix elements $D_x$ is shown as a function of the reciprocal vector, $\mathbf{k}$, in Fig. 3. The reciprocal vector is measured relative to the Weyl point, i.e., the coordinates of the Weyl point are $(0,0,0)$. Considering the dipole matrix element as a function of $k_x$ and $k_y$ at a fixed value of $k_z$, we can characterize its behavior as follows. At $k_z = 0$, the dipole matrix element is singular at the Weyl point. This singularity is exactly of the same type as the singularity of the interband dipole matrix element in graphene. For nonzero $k_z$ the system becomes similar to graphene with a gap. As a result, the dipole matrix element has two peaks (one is positive and another is negative) near the origin (Weyl point). The corresponding distribution of the dipole matrix element is shown in Fig. 3. For $k_z \neq 0$, the dipole matrix element has both real and imaginary parts.

Figure 4 shows the conduction band population near Weyl point $W_1$ as a function of a reciprocal vector at different moments of time. The residual conduction band population has two peaks, the positions of which are correlated with the positions of the peaks of the dipole matrix element, $D_x$, shown in Fig. 3.

The time evolution of CB population distribution can be understood from the intraband electron dynamics in the reciprocal space. Such dynamics is described by the acceleration theorem, Eq. (8). The electron wave vector follows the vector potential, $\propto \int^t F(t_1)dt_1$, see Eq. (8). Then, for $t < -15$ fs, the electric field moves electrons in the negative direction of axis $k_x$, i.e., the
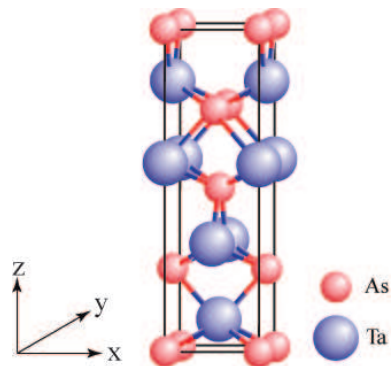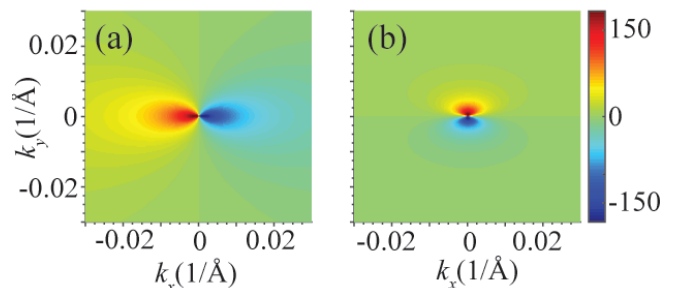


FIG. 3: (Color online) Interband dipole matrix element $D_x$ as a function of reciprocal vector $(k_x, k_y, 0.05)$ near the first Weyl point $W_1$. Both real (a) and imaginary (b) parts of $D_x$ are shown.
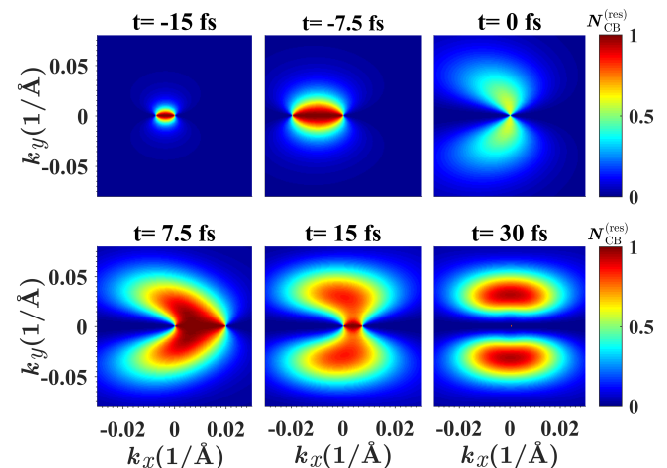


FIG. 4: (Color online) Conduction band population as a function of wave vector near the first Weyl point, $W_1$, at different moments of time. The results are shown for $x$ polarized pulse with the amplitude of $F_0 = 0.003$ (V/Å) and for $k_z = 0$ (1/Å).
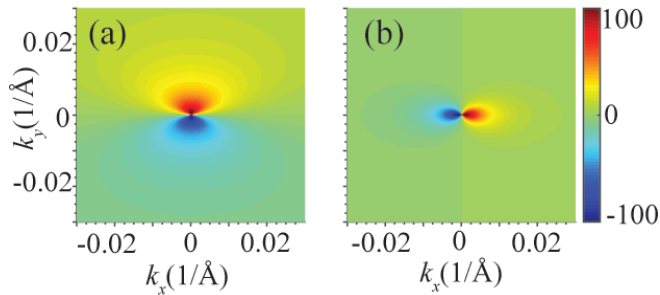
FIG. 5: (Color online) Interband dipole matrix element $D_y$ as a function of reciprocal vector $(k_x, k_y, 0.05)$ near the first Weyl point $W_1$. Both real (a) and imaginary (b) parts of $D_y$ are shown.



FIG. 6: (Color online) Conduction band population as a function of wave vector near the first Weyl point, $W_1$, at different moments of time. The results are shown for $y$ polarized pulse with the amplitude of $F_0 = 0.003$ (V/Å) and for $k_z = 0$ (1/Å).

vector potential is negative. During such motion the interband mixing of the conduction and valence band states is the strongest when an electron passes the region near the Weyl point, where the interband dipole matrix element is the largest. This behavior produces a hot spot with large CB population (almost 1) near the Weyl point at $t = -15$ fs (see Fig. 3). At $t > -15$ fs, the electrons move in the positive direction of axis $k_x$ and crosses again the region of Weyl point with large interband coupling. Such crossing transfers electrons from the conduction band into the valence band, resulting in small CB population at $t = 0$ fs when electrons return to their initial positions in the reciprocal space. At $t > 0$ fs, electrons continue their motion in the position direction of axis $k_x$, resulting again in large CB population, but now to the right from the Weyl point, at $t = 7.5$ fs. This population becomes small when electrons cross the region near the Weyl point the second time. Finally, at the end of the pulse, the CB population near the Weyl point becomes small, while it is large at some distance from the Weyl point, where a single passage does completely transfer an electron from the valence into the conduction bands. Such behavior is similar to what has been observed in graphene.

## B. y-polarized pulse

In this case the light is polarized along $y$ axis and is incident along the $z$ direction, see Fig.2. The profile of the dipole matrix element $D_y$ as a function of the reciprocal vector is similar to the one of $D_x$. At $k_z = 0$, the dipole matrix element $D_y$ as a function of $k_x$ and $k_y$ is singular at the Weyl point. At nonzero $k_z$, the dipole matrix element $D_y$ has two peaks near the origin $[(k_x, k_y) = (0,0)]$ - see Fig. 5. The only difference between $D_y$ and $D_x$ is that $D_y$ has a smaller magnitude, by $\approx 50\%$.

The conduction band population distribution for the Weyl point $W_1$ is shown in Fig. 6 at different moments
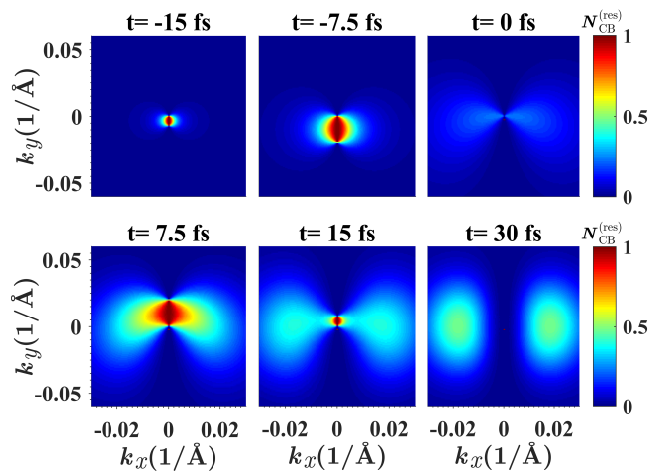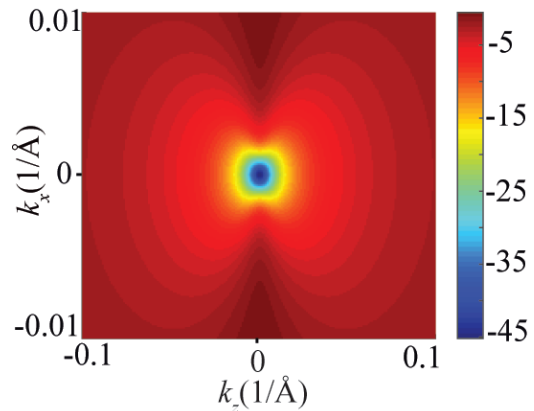


FIG. 7: (Color online) Interband dipole matrix element $D_z$ as a function of reciprocal vector $(k_x, 0, k_z)$ near the first Weyl point $W_1$. Only imaginary part of $D_z$ is shown. The real part is zero.

in time. Similar to $x$-polarized pule, the residual conduction band population has two well-pronounced maxima, which are at the same positions as the maxima of the dipole matrix element, $D_y$. This behavior is similar to the one observed for $x$-polarized light. The main difference is that, the maximum residual conduction band population for $y$-polarized light is almost two times smaller than the maximum conduction band population for $x$-polarized light. This is due to a smaller value of the corresponding interband dipole matrix element.
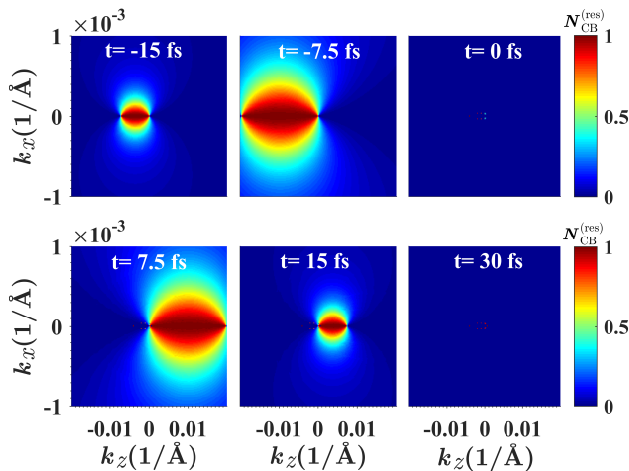
FIG. 8: (Color online) Conduction band population as a function of wave vector near the first Weyl point, $W_1$, at different moments of time. The results are shown for $z$ polarized pulse with the amplitude of $F_0 = 0.003$ (V/Å) and for $k_y = 0$ (1/Å).



FIG. 9: (Color online) Conduction band population as a function of wave vector near the second Weyl point, $W_2$, at different moments of time. The results are shown for $z$ polarized pulse with the amplitude of $F_0 = 0.003$ (V/Å) and for $k_y = 0$ (1/Å).

### C.   z-polarized pulse

The dependence of the interband dipole coupling on the reciprocal vector is determined by parameters of the effective Hamiltonian. The parameters of the Hamiltonian, which characterize the electron dynamics along $x$ and $y$ directions, are almost the same (see Table 1), which results in similar responses of the system to $x$ and $y$ polarized pulses. Along $z$ direction, the corresponding parameters of the Hamiltonian ($v_z$ and $v_{0z}$) are small, which strongly modifies the dipole matrix elements and the electron dynamics along $z$ direction. The dipole matrix element $D_z$ for the Weyl point $W_1$ is shown in Fig. 7. The dipole matrix element $D_z$ has a maximum at the Weyl point. This behavior is different from $D_x$ and $D_y$, which have two maxima near the Weyl point. This property of the dipole matrix element, $D_z$, determines the electron dynamics in the pulse polarized along $z$ axis. Here, we assume that the pulse propagates along $y$ direction, see Fig.2. The conduction band population distribution in the reciprocal space is shown in Fig. 8 for $W_1$ for the field amplitude of $F_0 = 0.003$ (V/Å). During the pulse, there is a large conduction band population near the Weyl point. Such large population is due to strong mixing of the valence and conduction band states when an electron passes the region of large interband coupling, which is near the Weyl point. The first passage of such region results in large conduction band population, while after the second passage the conduction band population becomes almost zero. Such cancellation of the conduction band population is the effect of destructive interference, which was also observed in graphene.

Finally the residual conduction band population becomes almost zero. This is a unique feature of Weyl point $W_1$, which is due to highly localized nature of the interband dipole coupling near the Weyl point. The strength of localization of the dipole matrix element depends on the corresponding parameters of the Hamiltonian. For Weyl point $W_2$, which has order of magnitude larger velocities $v_z$ and $v_{0z}$ (see Table 1), the residual conduction band population is relatively large and has two maxima near the Weyl point - see Fig. 9. Such conduction band population distribution is similar to the one for $x$ and $y$-polarized light.

### D.   Total occupation of the conduction band

Another important characteristic of electron dynamics in the field of the pulse is the total population of the conduction band, $\mathcal{N}_{CB}(t)$. The total CB population can be used to determine if the electron dynamics during the pulse is reversible or irreversible. If the electron dynamics is reversible then the residual CB population (CB population after the pulse) is much smaller than the CB population during the pulse, while if the electron dynamics is irreversible then the residual CB population is comparable to the maximum CB population during the pulse.

The total conduction band population as a function of time is shown in Fig. 10 for Weyl point $W_1$ and different pulse amplitudes. For $x$ and $y$ polarized pulses the electron dynamics is highly irreversible, which means that the residual conduction band population is comparable to the maximum conduction band population
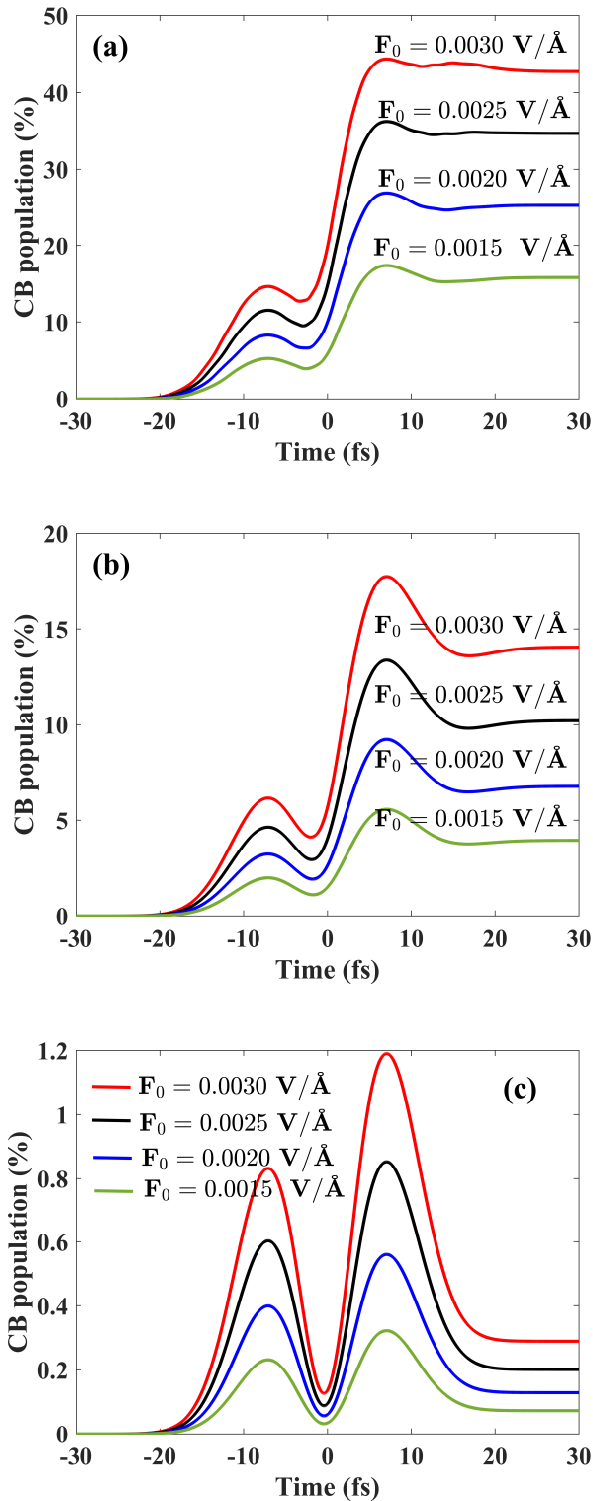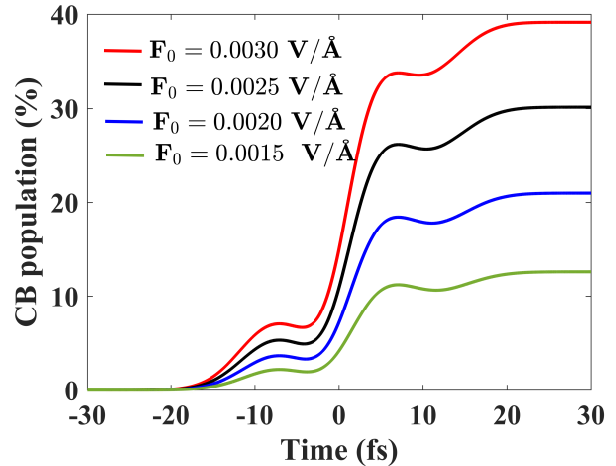
FIG. 11: (Color online) Total conduction band population as a function of time for the second Weyl point, $W_2$. The pulse is polarized along $z$ direction.



during the pulse [see Fig. 10(a,b)]. Such irreversible dynamics is similar to the electron dynamics in two dimensional (2D) materials such as graphene and phosphorene[23,24]. For $z$-polarized pulse the behavior is completely different [see Fig. 10(c)]. The electron dynamics in this case is highly reversible - the residual conduction band population is almost zero, which means that the system returns to its initial state. During the pulse, the conduction band population is relatively large. In all cases ($x$, $y$, and $z$ polarized pulses) the conduction band population monotonically increases with pulse amplitude.

For the second Weyl point, $W_2$, the electron dynamics for the $x$ and $y$ polarized pulses is similar to the one for the first Weyl point, $W_1$. The electron dynamics is irreversible and the residual conduction band population is comparable to the maximum conduction band population during the pulse. However, for $z$ polarized pulse, the electron dynamics for Weyl point $W_2$ is completely different from the electron dynamics for Weyl point $W_1$. For $z$ polarized pulse, the electron dynamics becomes highly irreversible - see Fig. 11.

Thus, the results for $z$ polarized pulse illustrate that the reversibility of electron dynamics is determined not only by the bandgap but also by the properties of interband dipole coupling.

The residual conduction band populations, $N_x^{(res)}$, $N_y^{(res)}$, and $N_z^{(res)}$, for the first Weyl point, $W_1$ are shown in Fig. 12 as a function of the pulse amplitude. The residual conduction band population for $z$ polarized pulse is almost zero for all values of $F_0$, which illustrates reversibility of electron dynamics along $z$ direction. For the $x$ and $y$ polarized pulses the residual conduction band population monotonically increases with $F_0$.

FIG. 10: (Color online) Total conduction band population as a function of time for the first Weyl point, $W_1$. The pulse is polarized along (a) $x$ (b) $y$ (c) $z$ directions.
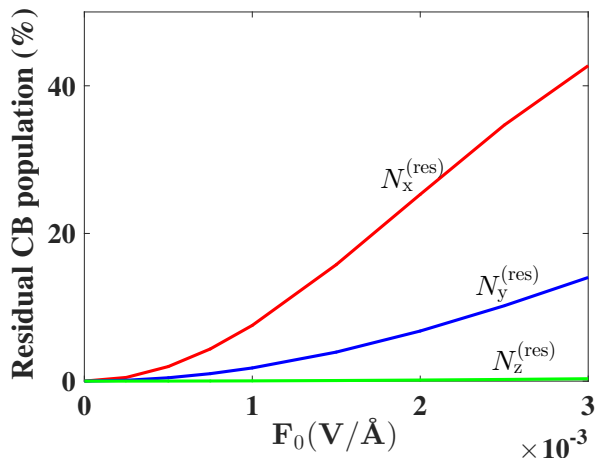
FIG. 12: (Color online) Residual conduction band populaion as a function of pulse amplitude, $F_0$, for the first Weyl point, $W_1$. The results are shown for the $x$ polarized ($N_x^{(res)}$), $y$ polarized ($N_y^{(res)}$), and $z$ polarized ($N_z^{(res)}$) pulses.

### E.    Transferred charge

Interband electron dynamics results in redistribution of electrons between the valence and conduction bands, while intraband dynamics determines the transport of electrons within a single band. Combination of these two types of dynamics results in generation of electric current, which can be found from Eq. (20). The current as a function of time is shown in Fig.13. The current itself has two contributions: interband and intraband. Our results show that the electric current is mainly determined by the intraband contribution. This can be also seen in Fig. 13, where both the current and the vector potential are shown. The results show that the current follows the vector potential. As we discussed in section II, the intraband electron dynamics is determined by the acceleration theorem and the corresponding electron momentum follows the vector potential. Then the intraband contribution to the current, which is proportional to electron group velocity, should also approximately follow the vector potential. At the same time, the interband contribution to the current is mainly determined by population of the conduction band, which follows the electric field of the pulse. Thus the interband contribution should mainly follow the electric field of the pulse but not the vector potential. Since the total current, shown in Fig. 13, follows the vector potential, then we can conclude that the total current is mainly determined by the intraband contribution. This is valid for all directions of pulse polarization.

With the known electric current, the charge transferred through the system can be calculated as an area under
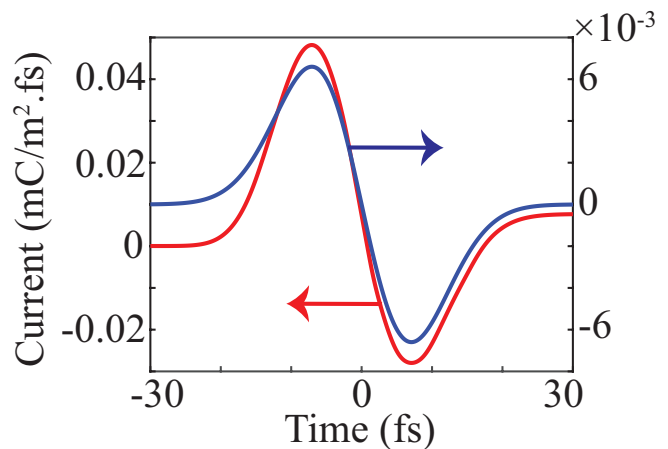


FIG. 13: (Color online) Current and vector potential , $\int F(t)dt$, as a function of time for $x$ polarized pulse with the amplitude of $F_0 = 0.001$ (V/Å). The results are shown for the first Weyl point, $W_1$.
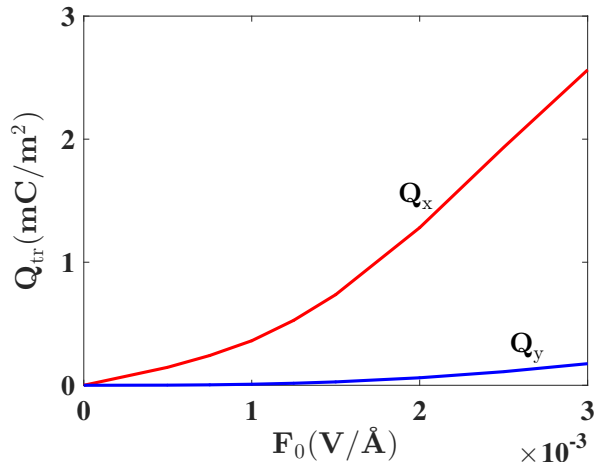


FIG. 14: (Color online) Transferred charge through Weyl semimetal as a function of pulse amplitude for the first Weyl point, $W_1$. The results are shown for $x$ polarized and $y$ polarized pulses.

the current versus time graph. The transferred charge as a function of field amplitude, $F_0$, is shown in Fig. 14 for the first Weyl point. Here $Q_x$ and $Q_y$ correspond to $x$ and $y$ polarized pulses, respectively. For $z$ polarized pulse, the transferred charge is almost zero. The transferred charges $Q_x$ and $Q_y$ monotonically increase with the field amplitude. The transferred charge for $y$ polarized pulse is almost fourteen times smaller than the transferred charge for $x$ polarized pulse. In all cases, the transferred charge is positive, which means that the direction of the transfer is the same as the direction of the field maximum. A non-zero transferred charge means that the electron dynamics in the field of the
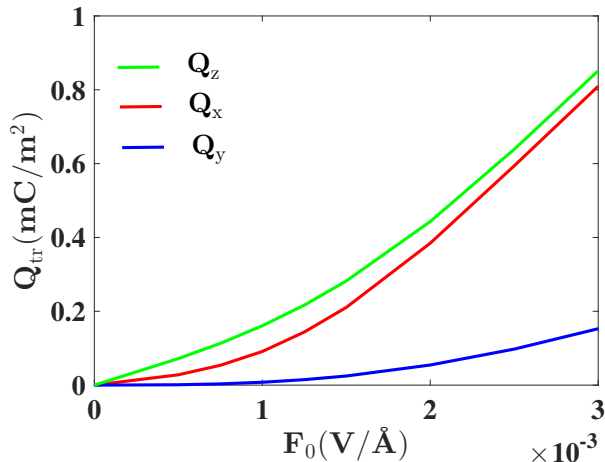
FIG. 15: (Color online) Charge transferred through Weyl semimetal for $x$ polarized pulse ($Q_x$), $y$ polarized pulse ($Q_y$), and $z$ polarized pulse ($Q_z$). The transferred charge is shown as a function of field amplitude for the second Weyl point, $W_2$.

pulse is highly non-linear. The direction of the charge transfer also depends on the carrier envelope phase of the pulse.

The transferred charge for the second Weyl point, $W_2$, is shown in Fig. 15. The transferred charge for $z$ polarized pulse is nonzero and is almost equal to the transferred charge for $x$ polarized pulse. For all directions of polarization, the transferred charge is positive and monotonically increases with field. The data also show that the transferred charges $Q_x$ and $Q_y$ for Weyl point $W_2$ is less than the corresponding charges for Weyl point $W_1$.

## IV. CONCLUSION

The Weyl semimetals have zero bandgap, which suggests that femtosecond dynamics of electrons in such materials should be highly irreversible, i.e., the residual electron population after the pulse is comparable to the conduction band population during the pulse. Such dynamics has been observed in graphene, which is a 2D version of Weyl semimetals. Our results show that irreversibility of ultrafast electron dynamics is determined not only by the bandgap of the material

but also by the profile and the magnitude of the inter-band dipole elements. We considered the case of TaAs Weyl semimetal, which has two sets of Weyl points. We found that for the first set of Weyl points, the electron dynamics is highly anisotropic. Namely, while for $x$ and $y$ polarized optical pulses the electron dynamics is irreversible, for $z$ polarized optical pulse the electron dynamics is highly reversible. For $z$ polarized optical pulse, the residual conduction band population is almost zero after the pulse. Such high reversibility is due to relatively small value of $z$ component of interband dipole matrix element and its high localization near the Weyl point. Although, in this case, the residual CB population is small, the maximum CB population during the pulse is large. Possibility of realization of reversible electron dynamics in gapless materials during femtosecond pulse is crucial for applications of laser pulses for femtosecond optical control of solids.

For the second set of Weyl point, the electron dynamics is irreversible for all directions of polarization of the optical pulse. In all cases, the residual conduction band population is comparable to the maximum conduction band population.

The femtosecond optical pulse also causes the charge transfer through the system during the pulse. The magnitude of the charge transfer strongly depends on the direction of polarization. For the first set of Weyl points, for $z$ polarized pulse, the transferred charge is almost zero. For $x$ and $y$ polarized pulses the charge is transferred in the direction of the pulse maximum. The magnitude of the transferred charge for $x$ polarized pulse is almost fourteen times larger than the magnitude of the transferred charge for $y$ polarized pulse.

For the second set of Weyl points, the charge is transferred through the system for all directions of polarization.

[1] R. Gattass and E. Mazur, Nature photonics **2**, 219 (2008).

[2] S.E. Kirkwood and Y.Y. Tsui, R. Fedosejevs, A.V. Brantov, and V.Y. Bychenkov, Phys. Rev. B **79**, 144120 (2009).

[3] E. Sie, C. Nyby, CD. Pemmaraju, Su. Park, X. Shen, J. Yang, M. Hoffmann, BK. Ofori-Okai, R. Li, A. Reid, Nature **565**, 61 (2019).

[4] G. Manzoni, A. Sterzi, A. Crepaldi, M. Diego, F. Cilento, M. Zacchigna, Ph. Bugnon, H. Berger, A. Ma-

grez, M. Grioni, F. Parmigiani, Phys. Rev. Lett. **115**, 207402 (2015).

[5] F. Nematollahi, V. Apalkov, and M. I. Stockman, Frontiers in Ultrafast Optics: Biomedical, Scientific, and Industrial Applications XIX **10908**, 1090803 (2019).

[6] M.S. Wismer, M.I. Stockman, and V.S. Yakovlev, Physical Review B **96**, 224301 (2017).

[7] Chris P. Weber, Bryan S. Berggren, Madison G. Masten, Thomas C. Ogloza, Skylar Deckoff-Jones, Julien Madéo, Michael K.L. Man, Keshav. M. Dani, Lingxiao Zhao, Genfu Chen, et al., Appl. Phys. **122**, 223102 (2017).

[8] T. Südmeyer, S. V. Marchese, S. Hashimoto, C. R. E Baer, G. Gingras, B. Witzel, and U. Keller, Nature Photonics **2**, 599 (2008).

[9] Tatiana. Itina and Nikita S. Shcheblanov, Book of abstracts, COLA 2011, 111 (2011).

[10] Jean-Yves. Bigot, Mircea. Vomir, and Eric. Beaurepaire, Nat. Phys. **5**, 515 (2009).

[11] M. Hajlaoui, J. Papalazarou, S. Mauchain, Z. Lantz, C. Moisan, G. Boschetto, W. Jiang, et al., Nano letters **12**, 3532-3536 (2012).

[12] J. P. Callan, A. M.-T. Kim, C. A. D. Roeser, and E. Mazur, Phys. Rev. B **97**, 073201 (2001).

[13] A V Mitrofanov, A J Verhoef, E E Evgenii, J. Lumeau, L. Glebov, A M Zheltikov, and A. Baltuška, Phys. Rev. Lett. **2**, 147401 (2011).

[19] V. Apalkov and M. I. Stockman, Phys. Rev. B **88**, 245438 (2013).

[15] O. Kwon, T. Paasch-Colberg, V. Apalkov, B.-K. Kim, J.-J. Kim, M. I. Stockman, and D. Kim, Sci. Rep. **6** (2016).

[16] A. Schiffrin, T. Paasch-Colberg, N. Karpowicz, V. Apalkov, D. Gerster, S. Muhlbrandt, M. Korbman, J. Reichert, M. Schultze, S. Holzner, Nature **493**, 70 (2012).

[17] M. Schultze, E. M. Bothschafter, A. Sommer, S. Holzner, W. Schweinberger, M. Fiess, M. Hofstetter, R. Kienberger, V. Apalkov, V. S. Yakovlev, M. I Stockman, ,

[18] Nature **493**, 75 (2013).

[18] F. Krausz and M. I. Stockman, Nat Photon **8**, 205 (2014).

[19] V. Apalkov and M. I. Stockman, Phys. Rev. B **88**, 245438 (2013).

[20] H. K. Kelardeh, V. Apalkov, and M. I. Stockman, Phys. Rev. B **90**, 085313 (2014).

[21] H. K. Kelardeh, V. Apalkov, and M. I. Stockman, Phys. Rev. B **92**, 045413 (2015).

[22] H. K. Kelardeh, V. Apalkov, and M. I. Stockman, Phys. Rev. B **93**, 155434 (2016).

[23] H. K. Kelardeh, V. Apalkov, and M. I. Stockman, Phys. Rev. B **91**, 0454391 (2015).

[24] F. Nematollahi, V. Apalkov, and M. I. Stockman, Phys. Rev. B **97**, 035407 (2018).

[25] H. Weyl, Zeitschrift für Physik **56**, 330 (1929).

[26] G. Xu, H. Weng, Z. Wang, X. Dai, and Z. Fang, Phys. Rev. Lett. **107**, 186806 (2011).

[27] H. Weng, C. Fang, Z. Fang, B. A. Bernevig, and X. Dai, Phys. Rev. X **5**, 011029 (2015).

[28] S.-M. Huang, S.-Y. Xu, I. Belopolski, C.-C. Lee, G. Chang, B. Wang, N. Alidoust, G. Bian, M. Neupane, C. Zhang, et al., Nature communications **6**, 7373 (2015).

[29] X. Wan, A. M. Turner, A. Vishwanath, and S. Y. Savrasov, Phys. Rev. B **83**, 205101 (2011).

[30] A. Schiffrin, T. Paasch-Colberg, N. Karpowicz, V. Apalkov, D. Gerster, S. Muhlbrandt, M. Korbman, J. Reichert, M. Schultze, S. Holzner, et al., Nature **507**, 386 (2014).

[31] X. Wan, A. M. Turner, A. Vishwanath, and S. Y. Savrasov, Phys. Rev. B **83**, 205101 (2011).

[32] W. V. Houston, Phys. Rev. **57**, 184 (1940).

[33] C.-C. Lee, S.-Y. Xu, S.-M. Huang, D. S. Sanchez, I. Belopolski, G. Chang, G. Bian, N. Alidoust, H. Zheng, M. Neupane, B. Wang, A. Bansil, M.Z. Hasan, H. Lin, Phys. Rev. B **92**, 235104 (2015).